Ultrafast Excited State Dynamics in 9,9 '-Bifluorenylidene

ARTICLE *in* THE JOURNAL OF PHYSICAL CHEMISTRY A · JULY 2014

Impact Factor: 2.69 · DOI: 10.1021/jp504391s · Source: PubMed

8 AUTHORS, INCLUDING:

Ismael A Heisler
University of East Anglia
48 PUBLICATIONS **540** CITATIONS
SEE PROFILE

Wesley R Browne
University of Groningen
209 PUBLICATIONS **4,736** CITATIONS
SEE PROFILE

Wybren J Buma
University of Amsterdam
184 PUBLICATIONS **2,445** CITATIONS
SEE PROFILE

Sander Woutersen
University of Amsterdam
103 PUBLICATIONS **4,303** CITATIONS
SEE PROFILE

THE JOURNAL OF PHYSICAL CHEMISTRY A

Article

pubs.acs.org/JPCA

Ultrafast Excited State Dynamics in 9,9′-Bifluorenylidene

Jamie Conyard,[†] Ismael A. Heisler,[†] Wesley R. Browne,[‡] Ben L. Feringa,[‡] Saeed Amirjalayer,*[,§,∥] Wybren Jan Buma,[§] Sander Woutersen,[§] and Stephen R. Meech*[,†]

[†]School of Chemistry, University of East Anglia, Norwich Research Park, Norwich NR4 7TJ, U.K.

[‡]Stratingh Institute for Chemistry, University of Groningen, Nijenborgh 4, 9747AG Groningen, The Netherlands

[§]Van't Hoff Institute for Molecular Sciences, University of Amsterdam, Science Park 904, 1098 XH Amsterdam, The Netherlands

[∥]Physical Institute and Center for Nanotechnology (CeNTech), Westfälische Wilhelms-Universität Münster, Wilhelm-Klemm-Straße 10, 48149 Münster, Germany

ABSTRACT: 9,9′-Bifluorenylidene has been proposed as an alternative and flexible electron acceptor in organic photovoltaic cells. Here we characterize its excited state properties and photokinetics, combining ultrafast fluorescence and transient IR measurements with quantum chemical calculations. The fluorescence decay is ultrafast (sub-100 fs) and remarkably independent of viscosity. This suggests that large scale structure change is not the primary relaxation mode. The ultrafast decay populates a dark state characterized by distinct vibrational and electronic spectra. This state decays with a 6 ps time constant to a hot ground state that ultimately populates the initial state with a 20 ps time constant; these times are also insensitive to solvent viscosity. No metastable intermediate structures are resolved in the photocycle after population of the dark state. The implications of these results for the operation of 9,9′-bifluorenylidene as an electron acceptor and as a potential molecular switch are discussed.

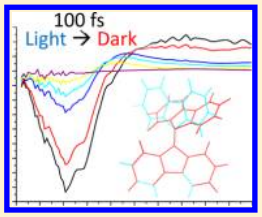

INTRODUCTION

A major objective for materials science is optimization of the performance of organic photovoltaic devices.[1,2] A widely used design of a photovoltaic cell exploits light-induced charge separation in a bulk heterojunction layer sandwiched between a metal electrode and a transparent oxide semiconductor.[3,4] Typically, the heterojunction layer comprises a hole conducting polymer as the chromophore and a dispersed electron acceptor. By far the most widely used electron acceptors are fullerene derivatives, because they offer both high electron affinity and good electron transport properties.[5] In efforts to optimize the performance of organic photovoltaics considerable effort has been devoted to tuning the physical and chemical properties of the polymer electron donor,[6,7] but there has been less progress in modifying the fullerene electron acceptors. Recently Brunetti et al. introduced a potential new generation of electron acceptors based on a 9,9′-bifluorenylidene (9,9′BF, Figure 1) backbone.[8] The attractive features of 9,9′BF are the wide range of sites for chemical functionalization, its favorable electron affinity (presumed to arise from structural relaxation of the strained neutral state on accepting an electron) and its suitable optical properties.[9−11] Here we use excited state dynamics as a surrogate for dynamics in the 9,9′BF anion. This is a reasonable choice given that excitation is localized on the ethylene double bond (see below) and, in the case of ethylene, the structural changes calculated to occur on electron attachment and electronic excitation are similar.[12−14] A direct study of dynamics following formation of the 9,9′BF anion is currently precluded, because sufficiently short-pulsed electron sources are not available. Chemical generation of the anion via a photoexcited electron transfer reaction is possible but would be too slow for the subpicosecond dynamics observed, as it would require either translational diffusion of reactants (nanoseconds) or structural reorganization of the medium (picoseconds).

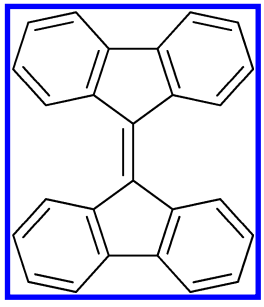

Figure 1. Chemical structure of 9,9′BF.

Here we report the excited state structural dynamics of 9,9′BF in a variety of solvents. We use ultrafast fluorescence spectroscopy to reveal an extraordinarily efficient sub-100 fs relaxation from the Franck−Condon excited electronic state. This relaxation is shown to occur via a volume conserving (solvent friction independent) mechanism, which has important consequences for the function of 9,9′BF in condensed media. Subsequent subpicosecond and picosecond dynamics on the excited state and ground state potential energy surfaces are probed by transient absorption spectroscopy in the visible and mid-infrared spectral regions. These data address the potential of 9,9′BF to act both as an electron acceptor in photovoltaics

Received: May 5, 2014
Revised: July 11, 2014
Published: July 15, 2014

dx.doi.org/10.1021/jp504391s | J. Phys. Chem. A 2014, 118, 5961−5968

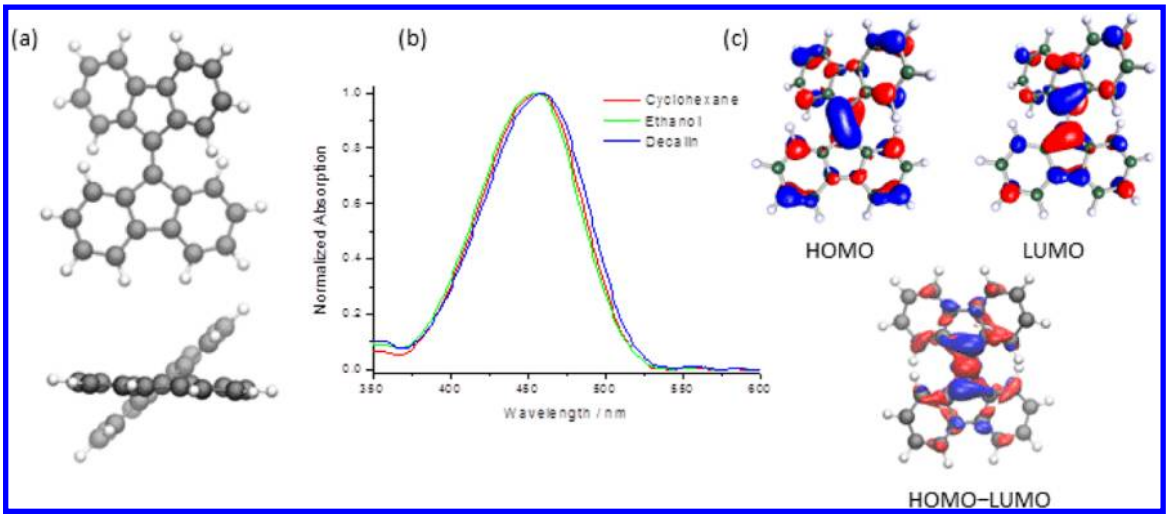

Figure 2. (a) Calculated geometry of 9,9′BF. (b) Electronic absorption spectra in three solvents. (c) Calculated HOMO, LUMO, and electron density difference plot between HOMO and LUMO (HOMO−LUMO).

and as a core unit for the development of a family of molecular switches to complement those based on the bistricyclic enes.[15,16]

EXPERIMENTAL SECTION

9,9′BF was synthesized as described earlier,[17] recrystallized from heptane, and characterized by ^{1}H NMR spectroscopy.

Time-resolved fluorescence measurements were recorded by fluorescence up-conversion using methods described elsewhere.[18] The laser was a 1 W source of 100 MHz 20 fs pulses at 800 nm. Fluorescence was excited by the second harmonic at 400 nm (7 mW) and up-converted in a 50 μm BBO crystal with the residual 800 nm beam. Resolution better than 50 fs was obtained by using all reflective optics and careful compensation of dispersion in both pump and gate beams. The data were analyzed by fitting to a sum of exponentials and damped oscillator functions, through deconvolution with the instrument response. The instrument response was measured by up-converting Raman scattered pump radiation. Analysis and fitting used an evolutionary fitting algorithm.[19]

Transient visible absorption used a 1 kHz 150 fs 800 nm source generating up to 300 μJ per pulse.[20] The pump pulse was generated by SHG at 400 nm. The probe pulse was a white light continuum generated in a continuously translated CaF_2 plate. The pump (<500 nJ/pulse) was chopped at 500 Hz to allow simultaneous collection of pump on and off traces and therefore generation of the transient difference spectra on a shot-by-shot basis. The data at discrete wavelengths were fit to sums of exponentials using the evolutionary fitting algorithm.

For the transient IR measurements, 400 nm pump and mid-IR probe pulses were generated using a Ti:sapphire laser (Spectra-Physics Hurricane, 600 μJ) with a repetition rate of 1 kHz. Similar to the transient absorption measurements, the pump pulse (400 nm) was generated by SHG. IR probe pulses were generated by difference frequency mixing of signal and idler from a BBO-based OPA (Spectra-Physics OPA-800C) in $AgGaS_2$. The delay positions were scanned by adjusting the beam-path of the UV pump using a Newport ESP300 translation stage. The temporal resolution of 200 fs was measured from the fwhm of the pump−probe cross-correlation function. Transient IR data were fit with a global least-squares method using a sequential model, with time constants $1/k_1$ and $1/k_2$ for first and second step, respectively. The total time dependent absorption change is then

$$\Delta a(\nu,t) = \Delta a_{S_1}(\nu)e^{-k_1 t} + \Delta a_{S_0^\ddagger}(\nu)\frac{k_1}{k_1 - k_2}(e^{-k_2 t} - e^{-k_1 t})$$

where it should be noted that the $\Delta\alpha_{S_1,S_0^\ddagger}(\nu)$ are species-associated absorption-difference spectra with respect to the S_0 state.

All quantum mechanical calculations were performed using the TURBOMOLE suite of programs.[21] For all elements the cc-pVDZ basis sets were employed.[22] TD-DFT calculations have been performed with the generalized gradient approximation functional BLYP[23,24] and with the hybrid-functional B3LYP.[25] Further, post-Hartree−Fock calculations were performed on the basis of spin-component scaled second-order Møller−Plesset perturbation theory[26] and the approximate coupled-cluster singles-and-doubles model CC2. All perturbation method calculations were performed using the resolution of identity (RI) approximation[27] and the efficient RICC2 module[28] implemented in the TURBOMOLE package together with the standard auxiliary basis sets.[29]

RESULTS AND ANALYSIS

9,9′BF comprises two nearly (but not exactly) planar fluorene units linked by a C9═C9′ double bond, which is twisted for steric reasons resulting in a structure with significant strain, and consequently an angle between the rings of 32° (Figure 2a). The electronic absorption spectrum of 9,9′BF exhibits a strong featureless transition with an onset at 525 nm and a maximum absorbance at 460 nm (Figure 2b). Neither the maximum wavelength nor the spectral shape are perturbed by changes in solvent, at least for the series cyclohexane (fluid nonpolar solvent), ethanol (polar and H-bonding), and decalin (viscous, nonpolar). The 460 nm absorption of 9,9′BF is considerably red-shifted from the structured 300 nm absorption of the parent fluorene, suggesting that the bridging C9═C9′ bond makes a major contribution to the spectrum; calculations show that electronic excitation is indeed localized on the ethylenic bridging bond (Figure 2c).

The steady state fluorescence of 9,9′BF in all three solvents is exceedingly weak and barely resolved above the solvent Raman

dx.doi.org/10.1021/jp504391s | J. Phys. Chem. A 2014, 118, 5961−5968

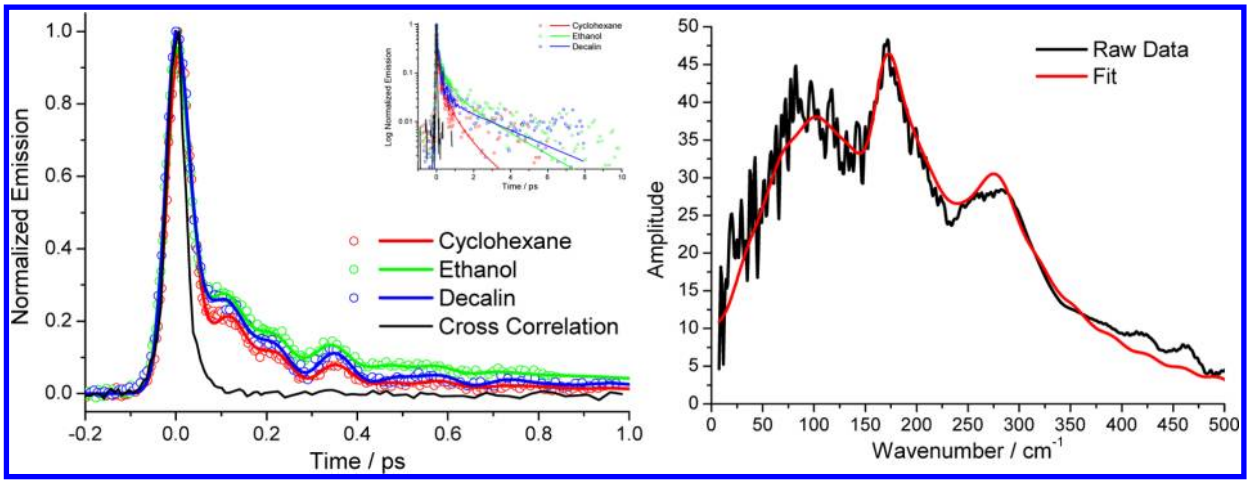

Figure 3. (a) Ultrafast fluorescence decay of 9,9′BF in three different solvents. The dominant fast decay is apparent, and the inset shows the relaxation is complete in 3 ps. The solid line is the instrument response (up-converted solvent Raman). (b) The oscillatory part of the decay was isolated and transformed to the frequency domain where it is compared with the Fourier transform of the oscillatory part of the fitted function. Three distinct vibrational modes are apparent in both traces.

Table 1. Analysis of Transient Fluorescence Data Analysed by Deconvolution Using the Scattered Raman as the Excitation Function and Eq 1 for the Fit: (a) Exponential Decay Kinetics; Reproducibility in the Fluorescence Lifetimes Recovered Better than 15%; (b) Oscillator Functions, Where the Frequencies Are Reproducible within 25%

(a) Fluorescence Decay

solvent	viscosity/mPa s	τ_1/ps	A_1	τ_2/ps	A_2	τ_3/ps	A_3	$\langle\tau\rangle$/ps
cyclohexane	0.89	0.09	0.91	0.48	0.08	1.56	0.01	0.13
ethanol	1.07	0.08	0.82	0.48	0.14	2.16	0.04	0.22
decalin	2.5	0.09	0.90	0.36	0.07	2.40	0.03	0.19

(b) Oscillatory Response

solvent	τ_{D1}/ps	ω_1/THz	$A_{\omega1}$	φ_1	τ_{D2}/ps	ω_2/THz	$A_{\omega2}$	φ_2	τ_{D3}/ps	ω_3/THz	$A_{\omega3}$	φ_3
cyclohexane	0.05	2.71	0.85	2.21	0.25	4.88	0.05	2.57	0.17	8.38	0.10	1.16
ethanol	0.06	2.83	0.79	2.05	0.19	4.88	0.11	2.72	0.20	8.38	0.10	1.18
decalin	0.06	2.70	0.78	2.07	0.27	4.98	0.09	2.43	0.19	8.17	0.13	1.45

background, suggesting a fluorescence quantum yield $<10^{-4}$. However, the time-resolved fluorescence signal in the up-conversion method is determined by the transition moment and not the quantum yield, so time-resolved fluorescence data with 50 fs resolution were readily collected[18] (Figure 3). Immediately apparent is the extremely fast fluorescence decay, which has a series of oscillations superimposed upon it. This complex decay pattern could be fitted by a minimum of a sum of three exponentially decaying components and three damped oscillations:

$$F(t) = \sum_{n=1}^{3} A_n e^{-t/\tau_n} + A_{\omega n} \sin(\omega_n t + \phi_n) e^{-t/\tau_{Dn}} \quad (1)$$

where the τ_n are fluorescence decay times and τ_D is the damping time of the oscillator of frequency ω and relative phase ϕ; fits are presented in Figure 3 and data in Table 1a,b. The fastest fluorescence decay time of ca. 90 fs is dominant, with a weight of 80−90%. The two longer lifetimes are of lower weight (<20%) and are in the range 0.4−2.4 ps, giving a mean fluorescence decay time of 180 ± 50 fs. Significantly, the fluorescence decay kinetics of 9,9′BF do not show a significant dependence on solvent polarity or viscosity (Table 1a).

Oscillations due to impulsive coherent excitation of vibrational modes are often observed in ultrafast spectroscopy. In transient absorption measurements the separation of excited state modes from ground state modes (excited through impulsive stimulated Raman scattering) is a difficult task requiring careful analysis of wavelength-resolved measurements of the transmission (or dispersion). In contrast, an oscillatory response in time-resolved fluorescence (Figure 3) can be unambiguously assigned to coherent excitation of vibrational modes in the excited electronic state that modulate the frequency and/or amplitude of the transition moment.[30−34] Three modes are recovered from the analysis, with the lowest frequency oscillator at 90 ± 20 cm^{-1} with τ_D = 60 fs, an intermediate frequency of low weight at 160 ± 30 cm^{-1} with 240 fs damping and a higher frequency response of 280 ± 40 cm^{-1} damped in 190 fs. Frequencies and damping times are also solvent independent (Table 1b). That the fitted frequencies accurately describe the model free experimental data is illustrated in the frequency domain spectrum (Figure 3b), which compares the Fourier transform of the raw data (with the sum of exponentials decay function subtracted) with that of the fitting function.

Ground state RIMP2 calculations reveal a number of low frequency modes between 40 and 200 cm^{-1} matching these excited state frequencies, including bridge bond torsion and pyramidalization and ring buckling modes. Given the localization of excitation on the double bond (Figure 2), it is likely that these mode frequencies will be shifted in the excited state, making a more definitive assignment of the observed excited state frequencies difficult. The correspondence between the 60

dx.doi.org/10.1021/jp504391s | J. Phys. Chem. A 2014, 118, 5961−5968

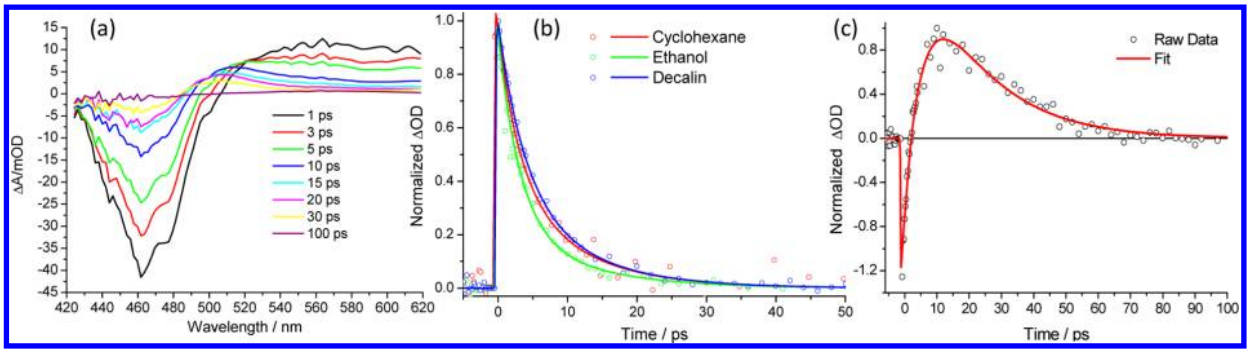

Figure 4. (a) Evolution of the transient absorption of 9,9′BF in decalin in the visible region of the spectrum. (b) Decay of transient absorption at 600 nm. (c) Intermediate kinetics at 520 nm.

fs damping of the 90 cm^{-1} mode and the 90 fs population lifetime may suggest its involvement in the reaction coordinate.[35] The less strongly damped higher frequency modes are more likely to be spectator modes, not strongly coupled to the reaction coordinate.

The lack of a solvent dependence in the population decay times, τ, is significant; in particular, it is noteworthy that the factor of 3 increase in viscosity between the otherwise similar solvents cyclohexane and decalin did not lead to any increase in decay time. Excitation localized on the C9═C9′ double bond is expected to reduce the bond order, allowing the release of steric strain through bond rotation, increasing the angle between the fluorene rings. Such large scale torsional motion involving groups as large as the fluorene ring is expected to be both slower than the subpicosecond mean relaxation time observed here and retarded by a viscous solvent. For an ultrafast reaction (Table 1a) a barrierless potential surface may be assumed, in which case the time scale for the rotation about the double bond will be reflected in the time scale for diffusive molecular reorientation. Calculations and measurements exist for diffusive reorientation of biphenyl and substituted anthracenes, which have volumes similar to those of fluorene. These precedents predict a decay time that is >10 ps and linearly dependent on viscosity (although very often a weaker viscosity dependence is observed experimentally). Both the much faster relaxation observed for 9,9′BF and the fact that this retardation is not observed in the present data (Figure 3, Table 1) suggests that large scale torsional motion is not the primary intermolecular reorganization responsible for ultrafast decay of the Franck–Condon state.[36−38] We also studied the steady state fluorescence of 9,9′BF as a function of temperature in ethanol from room temperature to 85 K. Only a minor (at most 5 fold) enhancement of the very weak fluorescence was observed even below the glass transition (97 K), in contrast to quite similar molecules (e.g., fluorene based rotary motors) which readily revealed a fluorescence enhancement >50 times at low temperature (unpublished). We conclude that the subpicosecond relaxation that suppresses fluorescence from the Franck–Condon excited state in 9,9′BF does not involve a large scale intramolecular structural reorganization. This result has functional significance. The observation of such a fast relaxation independent of medium friction suggests that the same ultrafast primary relaxation can occur even in the solid state, such as in the heterojunction layer of a photovoltaic cell; this structural relaxation may act to stabilize the electron acceptor.

Transient absorption experiments show that the Franck–Condon state does not decay directly back to the ground state (Figure 4). Within 0.5 ps (i.e., after the 100 fs decay of the Franck–Condon state) a new state (positive ΔOD) has been formed, absorbing above 540 nm. This new state has a broad electronic spectrum red-shifted with respect to the 450 nm ground state bleach. It decays in a non-single-exponential fashion (Figure 4b) with a 6 ps mean time constant (Table 2) to yield a transient absorption at 500 nm, which subsequently decays to repopulate the initial state (Figure 4c). The ground state repopulation at 460 nm is slower than the decay of the transient absorption and biexponential with 5 and 19 ps recovery times. As was found for the ultrafast fluorescence, these kinetics are independent of solvent, as shown in Figure 4b and the mean relaxation times (Table 2); the differences in the decalin data (Table 2b) reflect correlation among the individual amplitude and decay times in the fitting. Global analysis was applied to the spectra and also recovered two relaxation times, of 4.5 ± 2 ps and 16 ± 2 ps, with the longer component associated with the ground state recovery and 520 nm transient. This is in good agreement with the single wavelength analysis in Table 2. The global analysis also indicated that an additional longer component of small amplitude (a few percent) would be required for a complete fit. However, this most probably reflects a departure from first-order kinetics associated with a time dependent spectral shape and does not justify addition of an extra term.

Table 2. Exponential Fits to Transient Absorption Data in Three Solvents at (a) the Wavelength of the Red Shifted Transient 620 nm and (b) the Ground State Recovery (435 nm)[a]

solvent	τ_1/ps	A_1	τ_2/ps	A_2	$\langle\tau\rangle$/ps
		(a) 620 nm			
cyclohexane	3.28	0.63	11.34	0.37	6.25
ethanol	3.24	0.77	11.69	0.23	5.13
decalin	3.84	0.61	10.57	0.39	6.46
		(b) 435 nm			
cyclohexane	5.42	0.62	17.57	0.38	10.04
ethanol	4.99	0.60	17.61	0.40	10.00
decalin	4.28	0.29	12.32	0.71	10.01

[a]The weighted (by the pre-exponential factor) mean relaxation time is also shown in angle brackets. The reproducibility is 15%.

The transient IR difference spectrum (Figure 5) in the aromatic CC stretch region shows a combination of bleach modes (negative ΔOD), which arise from the ground state (e.g., 1450, 1480, and 1610 cm^{-1}). These are accompanied by instantaneously (i.e. within 300 fs) formed red-shifted transient

dx.doi.org/10.1021/jp504391s | J. Phys. Chem. A 2014, 118, 5961−5968

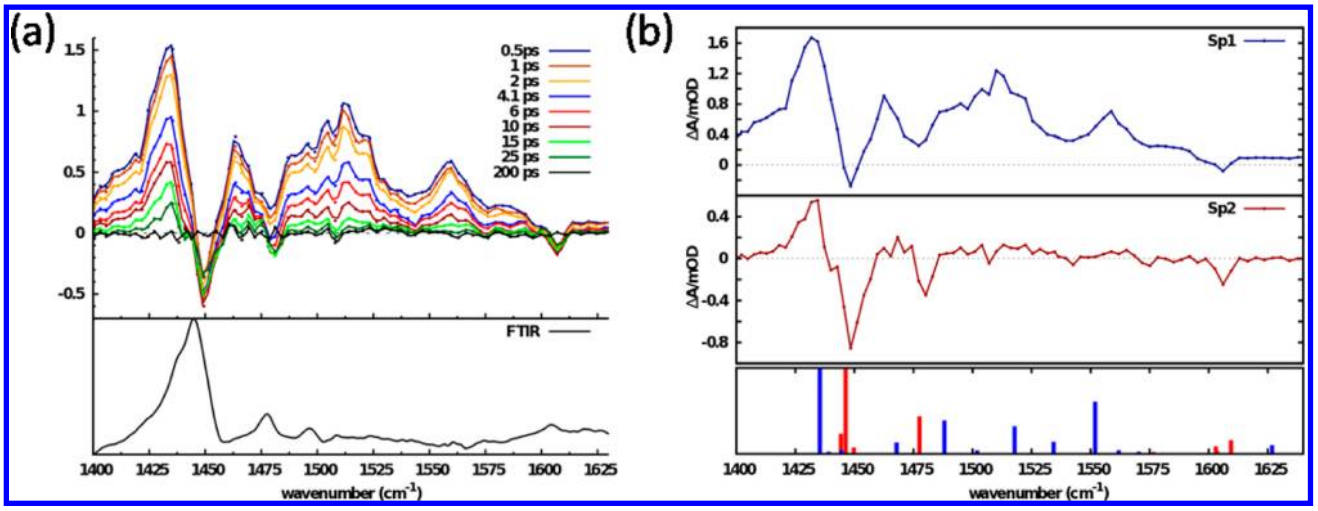

Figure 5. (a) Transient IR difference spectra of 9,9′BF. The corresponding steady state IR spectrum is shown in the lower panel. (b) Global analysis of transient IR spectra in terms of a biexponential model that recovers 5 ps (Sp1) and 21 ps (Sp2) components (top). Calculated IR spectra of the ground (red) and excited state (HOMO−1 → LUMO; low transition moment) (blue) on the BLYP-level (bottom).

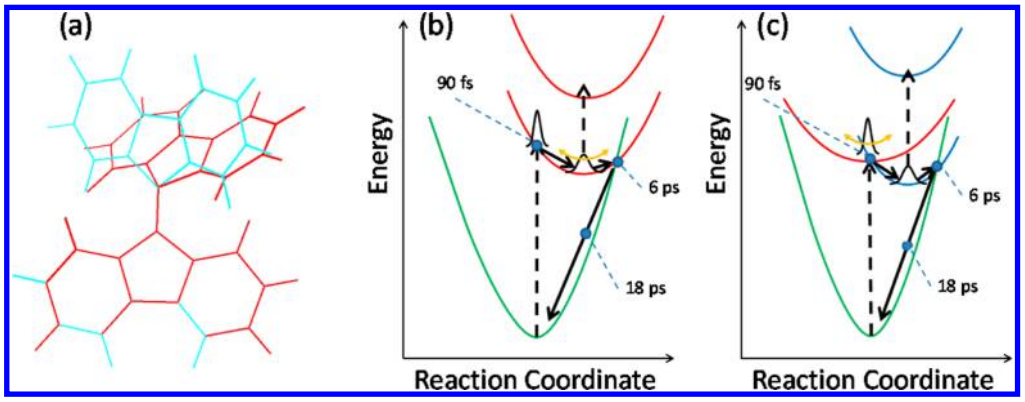

Figure 6. (a) Structure evolution for the single state model to yield a decrease in the transition moment from the Franck−Condon state consistent with experiment (torsion angle +10°, pyramidalization +30°). (b) Mechanism proposed for relaxation on a single excited state surface (red). Motion along the reaction coordinate occurs in 90 fs, and simultaneously excited state spectator modes are coherently excited (yellow). The dark state is observed in transient absorption to relax to the ground state in 6 ps, which cools in 18 ps. (c) Multistate model. The initially excited state (red) reaches a conical intersection near the FC state, where the major fraction of the population internally converts to a lower lying optically forbidden (dark) state (blue) in 90 fs. The remaining fraction stays on the bright state and decays in <1 ps (Figure 3) and supports excited state coherences (yellow). The dark state, which exhibits transient absorption, decays to a hot electronic ground state in 6 ps, which cools as in (b).

absorptions (1430 and 1460 cm^{-1}), which can be assigned to the corresponding modes in the excited state. Significantly, superimposed on these are broad transient absorptions at 1560 and 1520 cm^{-1}. There are no modes equivalent to these in the ground state bleach spectrum, so they are ascribed to a newly formed excited state appearing within 300 fs. These new absorptions suggest intensity borrowing due to vibronic coupling in the excited state.[39] The transient IR spectrum was subjected to a global kinetic analysis. The data were accurately described by a biexponential decay with time constants 5 and 21 ps, in line with the transient electronic spectra. The spectrum of the 5 ps component recovered from the global analysis is dominated by the induced transient absorptions, consistent with an assignment to an excited electronic state, whereas the 21 ps component reflects repopulation of the ground state (Figure 5b). The calculated IR spectra are in good agreement with the results obtained by the exponential fit of the experimental data (Figure 5b), confirming the kinetic model.

Combining all three data sets yields the following picture for the excited state dynamics of 9,9′BF. The Franck−Condon excited state relaxes on a 100 fs time scale populating a dark excited state. This primary excited state relaxation is the ultrafast barrierless release of strain around the bridging bond, involving volume conserving coordinates, such as pyramidalization and small scale double bond torsion. The resulting dark state is characterized by a broad red-shifted electronic absorption with a distinct vibrational spectrum. This state decays with a mean lifetime of 5−6 ps, presumably via a thermally accessible conical intersection, to populate a vibrationally "hot" electronic ground state, which itself relaxes within 20 ± 2 ps to the initial state (Figure 6). The ground state attained after internal conversion in 9,9′BF may initially be one of a number of possible conformers,[40] but none of these constitute a distinct metastable trap state, because the initial ground state is repopulated within 20 ps.

dx.doi.org/10.1021/jp504391s | J. Phys. Chem. A 2014, 118, 5961−5968

Table 3. Calculated Coordinate Dependent Energies and Transition Moments

(a) Vertical Excitation Energies E_{ex} (in eV), Transition Moments (in Parentheses) and Torsion Angle around the C=C Bond at the Ground State Geometry for Three Different Methods

	S_1 (HOMO−1→ LUMO)	S_2 (HOMO−2 → LUMO)	S_3 (HOMO → LUMO)	torsion angle/deg
BLYP/cc-pVDZ	2.13 (0.78×10^{-4})	2.14 (0.80×10^{-4})	2.33 (0.39)	35.95
B3LYP/cc-pVDZ	2.59 (0.20×10^{-3})	2.59 (0.40×10^{-3})	2.62 (0.46)	34.21
SCS-RICC2// RIMP2/cc-pVDZ	3.15 (0.12×10^{-3})	3.15 (0.29×10^{-5})	3.09 (0.59)	32.04

(b) Vertical Excitation Energies and Transition Moments of the Three Low Lying Electronic States Calculated for 9,9′BF by TDDFT (BLYP/cc-pVDZ) as a Function of Torsion and Torsion plus Pyramidalization Coordinates Starting from the Optimized Ground State Geometry

coordinates		S_1		S_2		S_3	
torsion	pyramid	E_{ex}/eV	osc str	E_{ex}/eV	osc str	E_{ex}/eV	osc str
35	15	2.08	0.96×10^{-2}	2.15	0.16×10^{-3}	2.32	0.34
35	30	1.85	0.11×10^{-1}	2.17	0.12×10^{-1}	2.19	0.19
35	45	1.59	0.34×10^{-1}	1.84	0.45×10^{-1}	2.11	0.66×10^{-3}
45	15	1.97	0.16×10^{-1}	2.05	0.45×10^{-3}	2.18	0.32
45	30	1.79	0.20×10^{-1}	2.08	0.99×10^{-1}	2.10	0.89×10^{-1}
45	45	1.67	0.12×10^{-1}	1.98	0.90×10^{-1}	2.12	0.20×10^{-2}

DISCUSSION

The nature of the reaction coordinate and the dark state in 9,9′BF are addressed through quantum chemical calculations. Pyramidalization and double bond torsion are considered as the reaction coordinates, and the evolution of the transition moment from excited to ground state is followed. The calculations suggest two related models for formation of the dark state, a single excited state evolving to a structure that has a negligible transition moment, or an internal conversion between a bright and a dark excited state, illustrated in Figure 6 and described below.

Although the TD-DFT calculations on both the BLYP and B3LYP levels differ in the ordering of the excited states compared to the RICC2 results, the character of the excited states and the energy difference between them is described accurately (Table 3), so that further studies on the TD-DFT level are reasonable to get a first idea of the relaxation mechanism. On this basis, excited and ground state energies as a function of twist and pyramidalization at the C=C bridge were followed using the BLYP functional. The initial excited state is unstable with respect to pyramidalization and twisting. We followed the energy and transition moment of the optically allowed (bright) state as a function of these two coordinates. For torsion alone the calculated decrease in transition moment is much smaller than Figure 2 requires (Table 3); the negligible contribution of the 5−6 ps dark state to the fluorescence allows for only a very small transition moment from the dark state. However, a combination of small torsion and large pyramidalization yields a very small transition moment, consistent with experimental observation. In this single state picture (Figure 6b), coherent dynamics on the excited state surface contribute to the observed oscillations in the fluorescence.[35] However, the structural distortion required between the final excited state and ground state is not small (Figure 6a) and might therefore be expected to be sensitive to solvent friction, which is not observed (Figure 3, Table 1). It was noted that in addition to the optically bright state the calculations predict two additional nearby electronic states with negligible oscillator strength (Table 3). This suggests the alternative possibility of a multistate relaxation pathway, in which internal conversion in 9,9′BF occurs between bright and dark excited electronic states (Figure 6c). Note that such a relaxation mechanism cannot be described within the framework of the TD-DFT calculations. In this model, population from the initially excited state reaches a CI via pyramidalization and torsional coordinates through which internal conversion to a lower lying dark state occurs. This dark state then decays via a second CI to the ground electronic state. The long-lived coherences in Figure 3 are not expected to survive passage and repassage through a CI, so in this picture the slower oscillatory components in the fluorescence represents a fraction of the population which remains on the initial bright state surface with its intensity modulated by the coherently excited spectator modes. These single and multipotential surface mechanisms are illustrated in Figure 6b,c.

The question as to whether an isomerization reaction takes place, crucial for the possible exploitation of 9,9′BF based molecules as molecular switches, will be revealed in future studies of asymmetrically substituted derivatives. However, the observed weak dependence on solvent viscosity suggests a minimal structural change during the photocycle, which is not optimal for many optical switch functions. On the other hand, the small structure change associated with dark state formation found here on optical excitation, but presumably also through electron transfer, may be a useful feature of 9,9′BF as an acceptor in photovoltaic cells.

CONCLUSIONS

The excited state dynamics of 9,9′BF were studied in detail through ultrafast time-resolved fluorescence and transient absorption in the visible and mid-IR regions. The primary relaxation step is extremely rapid (100 fs) and involves population of an intermediate (dark) state via motion along a coordinate that is volume conserving. Such a fast friction independent relaxation suggests that electron acceptors based on the 9,9′BF structure may be suitable for applications in solid phase bulk heterojunction photovoltaic devices. The nature of the excited state coordinate was investigated via DFT calculations and suggested involvement of pyramidialization and small scale fluorene ring torsion coordinates. However, multiple excited states were also detected and these may be involved in formation of the dark state. The subsequent decay of the intermediate state occurs on a picosecond time scale and can be modeled as a two-step relaxation, assigned to relaxation of the intermediate state to a hot ground state, which cools with a 20 ps time constant. The relaxation pathway in the ground state will be significant in assessing the role of these compounds

dx.doi.org/10.1021/jp504391s | J. Phys. Chem. A 2014, 118, 5961−5968

as molecular switches. This topic will be pursued in further studies of substituted 9,9′BF.

AUTHOR INFORMATION

Corresponding Authors

*S. Amirjalayer: e-mail, samir_01@uni-muenster.de.
*S. Meech: e-mail, s.meech@uea.ac.uk.

Notes

The authors declare no competing financial interest.

ACKNOWLEDGMENTS

S.R.M. thanks EPSRC (EP/H025715/1) for financial support. S.A. thanks the Deutsche Akademie der Naturforscher Leopoldina – German National Academy of Sciences for a Leopoldina research fellowship (grant number LPDS 2011-18). J.C. was supported by a studentship from UEA. W.R.B. and B.L.F. thank ERC for financial support (Starting Grant 279549 to W.R.B. and Advanced Investigator Grant 227897 to B.F. and financial support to J.C.).

REFERENCES

(1) Clarke, T. M.; Durrant, J. R. Charge Photogeneration in Organic Solar Cells. *Chem. Rev.* **2010**, *110*, 6736−6767.

(2) Bredas, J. L.; Norton, J. E.; Cornil, J.; Coropceanu, V. Molecular Understanding of Organic Solar Cells: The Challenges. *Acc. Chem. Res.* **2009**, *42*, 1691−1699.

(3) Yu, G.; Gao, J.; Hummelen, J. C.; Wudl, F.; Heeger, A. J. Polymer Photovoltaic Cells - Enhanced Efficiencies Via a Network of Internal Donor-Acceptor Heterojunctions. *Science* **1995**, *270*, 1789−1791.

(4) Park, S. H.; Roy, A.; Beaupre, S.; Cho, S.; Coates, N.; Moon, J. S.; Moses, D.; Leclerc, M.; Lee, K.; Heeger, A. J. Bulk heterojunction solar cells with internal quantum efficiency approaching 100%. *Nat. Photonics* **2009**, *3*, 297−302.

(5) Thompson, B. C.; Frechet, J. M. J. Organic photovoltaics - Polymer-fullerene composite solar cells. *Angew. Chem.-Int. Ed.* **2008**, *47*, 58−77.

(6) Bronstein, H.; Chen, Z. Y.; Ashraf, R. S.; Zhang, W. M.; Du, J. P.; Durrant, J. R.; Tuladhar, P. S.; Song, K.; Watkins, S. E.; Geerts, Y.; et al. Thieno 3,2-b thiophene-Diketopyrrolopyrrole-Containing Polymers for High-Performance Organic Field-Effect Transistors and Organic Photovoltaic Devices. *J. Am. Chem. Soc.* **2011**, *133*, 3272−3275.

(7) Ma, W. L.; Yang, C. Y.; Gong, X.; Lee, K.; Heeger, A. J. Thermally stable, efficient polymer solar cells with nanoscale control of the interpenetrating network morphology. *Adv. Funct. Mater.* **2005**, *15*, 1617−1622.

(8) Brunetti, F. G.; Gong, X.; Tong, M.; Heeger, A. J.; Wudl, F. Strain and Huckel Aromaticity: Driving Forces for a Promising New Generation of Electron Acceptors in Organic Electronics. *Angew. Chem.-Int. Ed.* **2010**, *49*, 532−536.

(9) Sun, G.-Y.; Li, H.-B.; Geng, Y.; Su, Z.-M. Potential of bifluorenylidene derivatives as nonfullerene small-molecule acceptor for heterojunction organic photovoltaics: a density functional theory study. *Theor. Chem. Acc.* **2012**, *131*, 1099.

(10) Sun, G.-Y.; Wu, S.-X.; Geng, Y.; Li, H.-B.; Wu, Y.; Su, Z.-M. Toward design of high-performance optoelectronic materials: comparative theoretical studies on the photophysical and charge transport properties of fluorene-based compounds. *Theor. Chem. Acc.* **2012**, *131*, 1176.

(11) Kim, H. U.; Kim, J.-H.; Suh, H.; Kwak, J.; Kim, D.; Grimsdale, A. C.; Yoon, S. C.; Hwang, D.-H. High open circuit voltage organic photovoltaic cells fabricated using 9,9 ′-bifluorenylidene as a non-fullerene type electron acceptor. *Chem. Commun.* **2013**, *49*, 10950−10952.

(12) Paddonrow, M. N.; Rondan, N. G.; Houk, K. N.; Jordan, K. D. Geometries of the Radical-Anions of Ethylene, Fluoroethylene, 1,1-Difluoroethylene, and Tetrafluoroethylene. *J. Am. Chem. Soc.* **1982**, *104*, 1143−1145.

(13) Hou, X. J.; Huang, M. B. Structures of the 1,1-difluoroethylene and tetrafluoroethylene anions. *J. Phys. Chem. A* **2002**, *106*, 10655−10662.

(14) Ben-Nun, M.; Quenneville, J.; Martinez, T. J. Ab initio multiple spawning: Photochemistry from first principles quantum molecular dynamics. *J. Phys. Chem. A* **2000**, *104*, 5161−5175.

(15) Browne, W. R.; Pollard, M. M.; de lange, B.; Meetsma, A.; Feringa, B. L. Reversible three-state switching of luminescence: A new twist to electro and photochromic behavior. *J. Am. Chem. Soc.* **2006**, *128*, 12412−12413.

(16) Chiu, C.-Y.; Wang, H.; Brunetti, F. G.; Wudl, F.; Hawker, C. J. Twisted but Conjugated: Building Blocks for Low Bandgap Polymers. *Angew. Chem.-Int. Ed.* **2014**, *53*, 3996−4000.

(17) Pollard, M. M.; Meetsma, A.; Feringa, B. L. A redesign of light-driven rotary molecular motors. *Org. Biomol. Chem.* **2008**, *6*, 507−512.

(18) Heisler, I. A.; Kondo, M.; Meech, S. R. Reactive Dynamics in Confined Liquids: Ultrafast Torsional Dynamics of Auramine O in Nanoconfined Water in Aerosol OT Reverse Micelles. *J. Phys. Chem. B* **2009**, *113*, 1623−1631.

(19) Zeidler, D.; Frey, S.; Kompa, K. L.; Motzkus, M. Evolutionary algorithms and their application to optimal control studies. *Phys. Rev. A* **2001** *64*, art. no.-023420.

(20) Lukacs, A.; Zhao, R. K.; Haigney, A.; Brust, R.; Greetham, G. M.; Towrie, M.; Tonge, P. J.; Meech, S. R. Excited State Structure and Dynamics of the Neutral and Anionic Flavin Radical Revealed by Ultrafast Transient Mid-IR to Visible Spectroscopy. *J. Phys. Chem. B* **2012**, *116*, 5810−5818.

(21) *Turbomole* V6.1, a Development of the University of Karlsruhe and Forschungszentrum Karlsruhe GmbH, 1989−2007, TURBOMOLE GmbH Since 2007, http://www.turbomole.com (accessed 6 July 2014).

(22) Wilson, A. K.; Woon, D. E.; Peterson, K. A.; Dunning, T. H. Gaussian basis sets for use in correlated molecular calculations. IX. The atoms gallium through krypton. *J. Chem. Phys.* **1999**, *110*, 7667−7676.

(23) Becke, A. D. Density-Functional Exchange-Energy Approximation With Correct Asymptotic-Behavior. *Phys. Rev. A* **1988**, *38*, 3098−3100.

(24) Lee, C. T.; Yang, W. T.; Parr, R. G. Development of the Colle-Salvetti Correlation-Energy Formula into a Functional of the Electron-Density. *Phys. Rev. B* **1988**, *37*, 785−789.

(25) Stephens, P. J.; Devlin, F. J.; Chabalowski, C. F.; Frisch, M. J. Ab-Initio Calculation of Vibrational Absorption and Circular-Dichroism Spectra Using Density-Functional Force-Fields. *J. Phys. Chem.* **1994**, *98*, 11623−11627.

(26) Grimme, S. Improved second-order Møller-Plesset perturbation theory by separate scaling of parallel- and antiparallel-spin pair correlation energies. *J. Chem. Phys.* **2003**, *118*, 9095−9102.

(27) Eichkorn, K.; Weigend, F.; Treutler, O.; Ahlrichs, R. Auxiliary basis sets for main row atoms and transition metals and their use to approximate Coulomb potentials. *Theor. Chem. Acc.* **1997**, *97*, 119−124.

(28) Hattig, C.; Weigend, F. CC2 excitation energy calculations on large molecules using the resolution of the identity approximation. *J. Chem. Phys.* **2000**, *113*, 5154−5161.

(29) Weigend, F.; Kohn, A.; Hattig, C. Efficient use of the correlation consistent basis sets in resolution of the identity MP2 calculations. *J. Chem. Phys.* **2002**, *116*, 3175−3183.

(30) Mokhtari, A.; Chebira, A.; Chesnoy, J. Subpicosecond Fluorescence Dynamics of Dye Molecules. *J. Opt. Soc. Am. B-Opt. Phys.* **1990**, *7*, 1551−1557.

(31) Pollard, W. T.; Lee, S. Y.; Mathies, R. A. Wave Packet Theory of Dynamic Absorption-Spectra in Femtosecond Pump-Probe Experiments. *J. Chem. Phys.* **1990**, *92*, 4012−4029.

(32) McClure, S. D.; Turner, D. B.; Arpin, P. C.; Mirkovic, T.; Scholes, G. D. Coherent Oscillations in the PC577 Cryptophyte Antenna Occur in the Excited Electronic State. *J. Phys. Chem. B* **2014**, *118*, 1296−1308.

(33) Chesnoy, J.; Mokhtari, A. Resonant Impulsive-Stimulated Raman-Scattering On Malachite Green. *Phys. Rev. A* **1988**, *38*, 3566−3576.
(34) Mokhtari, A. E.; Chesnoy, J. Terahertz Fluorescence Quantum Beats in a Dye Solution. *IEEE J. Quantum Electron.* **1989**, *25*, 2528−2531.
(35) Conyard, J.; Addison, K.; Heisler, I. A.; Cnossen, A.; Browne, W. R.; Feringa, B. L.; Meech, S. R. Ultrafast dynamics in the power stroke of a molecular rotary motor. *Nat. Chem.* **2012**, *4*, 547−551.
(36) Hartman, R. S.; Konitsky, W. M.; Waldeck, D. H.; Chang, Y. J.; Castner, E. W. Probing solute-solvent electrostatic interactions: Rotational diffusion studies of 9,10-disubstituted anthracenes. *J. Chem. Phys.* **1997**, *106*, 7920−7930.
(37) Nikowa, L.; Schwarzer, D.; Troe, J.; Schroeder, J. Viscosity and Solvent Dependence of Low-Barrier Processes - Photoisomerization of Cis-Stilbene in Compressed Liquid Solvents. *J. Chem. Phys.* **1992**, *97*, 4827−4835.
(38) Deeg, F. W.; Stankus, J. J.; Greenfield, S. R.; Newell, V. J.; Fayer, M. D. Anisotropic Reorientational Relaxation Of Biphenyl - Transient Grating Optical Kerr Effect Measurements. *J. Chem. Phys.* **1989**, *90*, 6893−6902.
(39) Nafie, L. A. Theory of vibrational circular dichroism and infrared absorption: Extension to molecules with low-lying excited electronic states. *J. Phys. Chem. A* **2004**, *108*, 7222−7231.
(40) Biedermann, P. U.; Stezowski, J. J.; Agranat, I. Polymorphism versus thermochromism: Interrelation of color and conformation in overcrowded bistricyclic aromatic enes. *Chem.—Eur. J.* **2006**, *12*, 3345−3354.